

Magnetic induced/enhanced coarsening in thin films

R. Backofen¹ and A. Voigt^{1,2}

¹*Institute of Scientific Computing, Technische Universität Dresden, 01062 Dresden, Germany*

²*Dresden Center for Computational Materials Science (DCMS), 01062 Dresden, Germany*

External magnetic fields allow to influence the microstructure in polycrystalline materials. Using a phase-field-crystal model we explore the influence on long time scaling and various geometrical and topological properties of grain structures in thin films. For parameters which lead to stagnant coarsening without magnetic fields, we observe two different linear scaling regimes if a magnetic field is considered. In the first the scaling exponent depends on the strength of magnetic interaction. After sufficient coarsening the texture becomes dominated by grains with their easy axis aligned to the magnetic field. This leads to an increase of low angle grain boundaries, reduces the influence of the magnetic field and leads to a second linear scaling regime with the exponent independent on the magnetic field. We further study the influence of the magnetic field on the grain size distribution (GSD), next neighbor distribution (NND) as well as grain shape and orientation and compare, if possible, with experimental results.

I. INTRODUCTION

Grain boundaries in polycrystalline materials are of paramount importance to various fields of science and engineering and are intensively studied theoretically and experimentally over decades. While quantitative comparison of geometrical and topological properties between theory/simulation and experimental data are still unsatisfactory in general, progress could be made for nanocrystalline thin metallic films, where geometric and topological characteristics of the grain structure could be shown to be universal and independent of many experimental conditions [1] and a phase field crystal (PFC) model [2, 3], which considers the essential atomic details but operates on diffusive time scales, was able to reproduce the universal grain size distribution and showed similar scaling properties and stagnation as in the experiments [4]. This is in contrast with more classical Mullins-like models, which only consider the evolution of the continuous grain boundary network [5]. Theoretical predictions and simulations for this type of models lead to self-similar structures and coarsening laws for the average grain size of the form t^α , with $\alpha = 1$ in the original setting [6]. Introducing retarding or pinning forces on the grain boundary in these models [7–9], or grain rotation [10–12] can also lower the scaling exponent and lead to stagnation. However, also these modifications are unable to reproduce the universal grain size distribution. A detailed comparison between these models with the PFC simulations [4] and the experiments in [1] can be found in [13]. With the achieved agreement for various geometrical and topological properties it is now time to use the PFC model as a predictive tool to control grain growth in thin films under the influence of external fields.

External magnetic fields during processing have been shown to influence grain growth and proposed as an additional degree of freedom to control the grain structure, see [14, 15] for reviews. The PFC model was extended to include magnetic interactions in [16, 17] and this extended version was used in [18] to explain the complex

interactions between magnetic fields and solid-state matter transport. It was shown that an applied magnetic field can increase the coarsening rate in grain growth, due to the lower energy of grains with their easy axis in line with the applied field. It was also shown that the mobility of grain boundaries is anisotropic with respect to the applied magnetic field. This kinetic effect leads to elongated grains. Applied magnetic fields lead to elastic reactions of the crystal (magnetostriction) and additionally to the formation of preferred diffusion paths which influence the grain boundary mobility. These effects already on short times influence the grain structure. In this paper we analyze the long time scaling behavior and various geometrical and topological properties in grain growth under the influence of a strong external magnetic field. The paper is organized as follows: We first review the underlying PFC model, the physical setting and the considered numerical approach. Then we consider the coarsening regime and analyze various geometrical and topological measures. Finally, we discuss the results, explain our findings and draw conclusions.

II. MODEL AND NUMERICAL APPROACH

The model in [16–18] combines the rescaled number density φ of the original PFC model [2, 3] with a mean field approximation for the averaged magnetization \mathbf{m} . The energy $\mathcal{F}[\varphi, \mathbf{m}] = \int f_{\text{PFC}}(\varphi) + \omega_B f_{\mathbf{m}}(\mathbf{m}) + \omega_m f_c(\varphi, \mathbf{m}) \, d\mathbf{r}$ with

$$\begin{aligned} f_{\text{PFC}}(\varphi) &= \frac{1}{2}\varphi(\mathbf{r})^2 - \frac{t}{6}\varphi(\mathbf{r})^3 + \frac{v}{12}\varphi(\mathbf{r})^4 \\ &\quad - \frac{1}{2}\varphi(\mathbf{r}) \int C_2(\mathbf{r} - \mathbf{r}')\varphi(\mathbf{r}') \, d\mathbf{r}' \\ f_{\mathbf{m}}(\mathbf{m}) &= \frac{W_0^2}{2}(\nabla \cdot \mathbf{m})^2 + r_m \frac{\mathbf{m}^2}{2} + \gamma_m \frac{\mathbf{m}^4}{4} - \mathbf{m} \cdot \mathbf{B} + \frac{\mathbf{B}^2}{2} \\ f_c(\varphi, \mathbf{m}) &= -\omega_m \varphi^2 \frac{\mathbf{m}^2}{2} - \sum_{j=1}^2 \frac{\alpha_{2j}}{2j} (\mathbf{m} \cdot \nabla \varphi)^{2j}, \end{aligned}$$

consists of contributions related to local ordering of the crystal, to local orientation of the magnetic moment and to coupling between crystal structure and magnetization. ω_B is a parameter to control the influence of the magnetic energy.

In order to maximize the anisotropy, as in [18], a square ordering of the crystal is preferred, which is realized within the XPFC formulation for $f_{\text{PFC}}(\varphi)$, see [19, 20]. The correlation function C_2 is approximated in k-space as the envelope of a set of gaussians and with peaks chosen by the primary k-vectors defining the crystal structure. For a square symmetry a minimum of two peaks is needed, $\hat{C}_2(\mathbf{k}) = \max(\hat{C}_{2,0}(\mathbf{k}), \hat{C}_{2,1}(\mathbf{k}))$ and $\hat{C}_{2,i}(\mathbf{k}) = A_i \exp[(\mathbf{k}_i - \mathbf{k})^2 / (2\xi_i^2)]$. The effect of temperature on the elastic properties is seen in the width of the peaks and modeled by ξ_i . A_i is a Debye-Waller factor controlling the height of the peaks. In order to increase numerical stability, short wavelength in the solutions of the density are gradually damped in k-space by adding $-10^{-6}(2\mathbf{k}_1 - \mathbf{k})^2$ to $C_k(\mathbf{k})$.

Magnetization in an isotropic and homogenous material is modeled by $f_m(\mathbf{m})$. The last two terms describe the interaction of the magnetization with an external and a self-induced magnetic field, \mathbf{B}_{ext} and \mathbf{B}_{ind} , respectively. The magnetic field is defined as $\mathbf{B} = \mathbf{B}_{\text{ext}} + \mathbf{B}_{\text{ind}}$, where \mathbf{B}_{ind} is defined with help of the vector potential: $\mathbf{B}_{\text{ind}} = \nabla \times \mathbf{A}$ and $\nabla^2 \mathbf{A} = -\nabla \times \mathbf{m}$.

The magnetic anisotropy of the material is due to the crystalline structure of the material. Thus, the magnetization has to depend on the local structure represented by φ and vice versa. The first term in $f_c(\varphi, \mathbf{m})$, changes the ferromagnetic transition in the magnetic free energy. On average φ^2 is larger in the crystal than in the homogeneous phase. Thus, ω_m and r_m can be chosen to realize a paramagnetic homogeneous phase and a ferromagnetic crystal. The second term depends on average on the relative orientation of the crystalline structure with respect to the magnetization.

The number density φ evolves according to conserved dynamics and magnetization according to non-conserved dynamics,

$$(1) \quad \frac{\partial \varphi}{\partial t} = M_n \nabla^2 \frac{\delta \mathcal{F}[\varphi, \mathbf{m}]}{\delta \varphi}, \quad \frac{\partial m_i}{\partial t} = -M_m \frac{\delta \mathcal{F}[\varphi, \mathbf{m}]}{\delta m_i}$$

$i = 1, 2$, respectively. However, in the limit of strong external magnetic fields, \mathbf{B}_{ext} , the magnetization, \mathbf{m} , can assumed to be homogeneous in the crystal. As shown in [18] the magnetization becomes perfectly aligned with the external magnetic field and independent on the relative orientation of the crystal. For paramagnetic or ferromagnetic materials near the Curie temperature, the magnitude of the magnetization $m = |\mathbf{m}|$ depends on the magnitude of the external magnetic field \mathbf{B}_{ext} . In this limit $f_m(\mathbf{m})$ is constant and does not influence the dynamics, and $\omega_m = 0$, as we are only concerned with the crystal phase. The remaining parameters are chosen as in Table I and lead to a minimization of the energy if the magnetization is aligned with the $\langle 11 \rangle$ -directions of the

t	v	M_n	$\bar{\varphi}$	$k_{0/1}$	$\xi_{1/2}$	$A_{0,1}$	ω_B	$\alpha_{2,4}$
1	1	1	0.05	$(2\pi, \sqrt{2}2\pi)$	(1, 1)	(1, 1)	1	(-0.001, 0)

TABLE I. Modeling parameters. The parameters are inspired by [20] and chosen to maximize the energetic difference between square and triangular phase.

crystal (easy axis). The hard axis are the $\langle 10 \rangle$ -directions. Due to the direct relation between \mathbf{B}_{ext} and \mathbf{m} , only the evolution equation for φ remains and reads

$$(2) \quad \frac{\partial \varphi}{\partial t} = M_n \nabla^2 \left[\varphi - \frac{t}{2} \varphi^2 + \frac{v}{3} \varphi^3 - \int C_2(\mathbf{r} - \mathbf{r}') \varphi(\mathbf{r}') d\mathbf{r}' + \omega_B \nabla \sum_{j=1}^2 \alpha_{2j} (\mathbf{m} \nabla \varphi)^{2j-1} \mathbf{m} \right]$$

where \mathbf{m} is considered as a parameter. Increasing \mathbf{m} leads to increasing anisotropy and magnetostriction [18]. The external magnetic field \mathbf{B}_{ext} and thus \mathbf{m} is assumed to be parallel to the thin film and the magnitude m is varied between [0; 0.8].

The evolution equation is solved semi-implicitly in time with a pseudo-spectral method. For numerical details we refer to [21, 22]. The reduced model eq. (2) is numerically more stable and less costly compared to the full model eq. (1). The timestep may be increased by an order of magnitude, making coarsening simulations for long times feasible.

We choose a parameter set, which shows stagnation in coarsening to include the effect of retarding forces and reflect the experimental finding. The simulation domain has size $L^2 = 819.2^2$. The mean particle distance is one and resolved by ten grid points, ($dx=0.1$). A time step of $dt=0.1$ was used. The magnetic moments \mathbf{m} are fixed along the x-direction.

III. COARSENING

Eq. (2), is used to model magnetic assisted annealing of thin films. The texture of the polycrystalline structure is monitored during annealing in order to extract geometrical and topological properties over time and compare them for different magnitudes m . To generate an appropriate initial condition we set $\mathbf{m} = 0$, start with a randomly perturbed density field φ and solve eq. (2) until we reach a polycrystalline structure with small crystallites with square symmetry. This configuration is used as initial condition for all simulations.

A. Scaling

Fig. 1 shows the evolution of the mean grain size with time, which increases with time and m . In all cases a linear scaling regime Fig. 1(B) is reached after an initial phase Fig. 1(A). Without magnetic impact a scaling of $\alpha = 1/3$ is observed. Increasing the magnetic impact increase the linear scaling. The maximum scaling $\alpha = 1$ is achieved for $m = 0.8$. However, this linear scaling regime ends and either turns into stagnation Fig. 1(C), which is observed without magnetic field and for small fields below some threshold. Above this threshold, here $m \geq 0.5$, the scaling becomes independent on magnetic interaction, with $\alpha = 1/3$, Fig. 1(D).

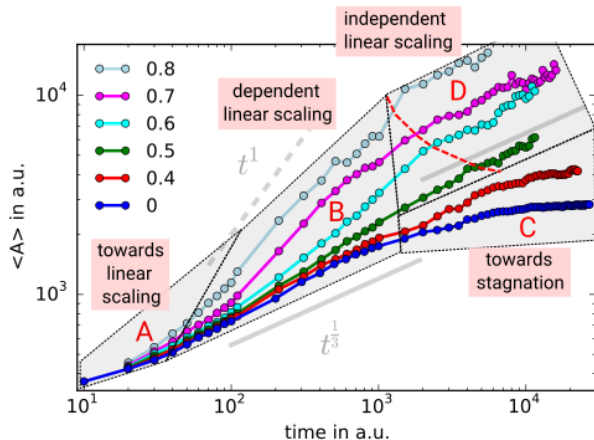


FIG. 1. Long time scaling behavior for different magnetic fields m . Four different regimes are identified: (A) towards linear scaling, an initial phase; (B) dependent linear scaling, a magnetically enhanced scaling regime with the scaling exponent depending on m ; (C) towards stagnation, a regime which is only present without or with low magnetic fields; and (D) independent linear scaling, a regime reached at late times, with a constant scaling exponent. m is varied between $[0; 0.8]$.

While the scaling exponents, the threshold and the transition region certainly depend on the chosen parameters, the characteristics of the scaling behavior with an initial accelerated coarsening regime (A), a linear scaling regime dependent on the magnetic driving force (B), a linear scaling regime independent on the magnetic driving forces (D) and a stagnation regime (C), are probably general.

B. Orientation selection

The magnetic driving force leads to preferable growth of grains, which are aligned with the easy axis, on the expense of the others. Fig. 2 shows typical orientation distributions and how they evolve over time under the influence of different magnitudes m . The color represents the local crystal orientation, θ , with $\theta = 0$ corresponding

to an aligned crystal orientation with the easy axis. Due to symmetry, $\theta \in [-0.25\pi, 0.25\pi]$. The initial orientation distribution is homogeneous, Fig. 2(a,b). Without a magnetic driving force $m = 0$ the orientation distribution stays homogeneous, Fig. 2(c,d,e). With a magnetic driving force this changes and a preferential growth of well aligned grains can be observed, Fig. 2(f,g,i,j). Grains with $\theta \approx 0$ (green) grow on the expense of the other grains (blue, red). As already quantified in Fig. 1, also the enhanced grain growth with increasing m can be seen by larger grain sizes for increasing m , Fig. 2(d,g,j). However, we are here interested in the orientation distribution, which becomes sharply peaked at $\theta = 0$, Fig. 2(e,h,k). The effect increases with increasing magnetic driving force m , as already analyzed also for the full model eq. (1) in [18].

The narrowing in orientation distribution has an effect on the impact of the external magnetic field. As it reduces the mean orientation difference of adjacent grains it also reduces the magnetic driving force. To measure this effect we define the mean magnetic driving force as the average energy difference due to magnetic anisotropy w.r.t. a perfectly aligned crystal. Fig. 3 shows this quantity over time. Initially the mean magnetic driving force strongly depends on the strength of the magnetic field. Large m lead to large driving forces. But over time the mean magnetic driving force decreases as the mean orientation deviation from a perfectly aligned crystal decreases due to grain selection. The strength of this effect correlates with the strength of the magnetic field. At large times, the mean magnetic driving force falls below a threshold. This large time behavior correlates with the independent scaling regime in Fig. 1(D), which occurs, when the mean magnetic driving force falls below $\approx 0.7 \cdot 10^{-4}$. The time this threshold is reached depends on m and is indicated by the dashed (red) line in Fig. 1. In the case of stagnation, $m < 0.5$, the mean magnetic driving force never exceeds the defined threshold.

C. Grain Size Distribution

The external magnetic field does not only change the orientation distribution but also the grain size distribution (GSD). Without external magnetic fields it was shown that the coarsening becomes self similar and the GSD is well described by a log-normal distribution [4]. We calculate the GSD for all coarsening simulations and fit log-normal distributions to our results. In Fig. 4 the two values defining the log-normal distribution, $\exp(\mu)$ and σ are shown over time. During the linear dependent (magnetic enhanced) scaling, Fig. 1(B), $\exp(\mu)$ and σ change, $\exp(\mu)$ decreases, while σ increases. Thus, the GSD is not constant over time and the coarsening not self similar. Only within the independent linear scaling regime, Fig. 1(D), the GSD becomes stationary on average and self similar growth is achieved.

As the number of grains is drastically decreased within

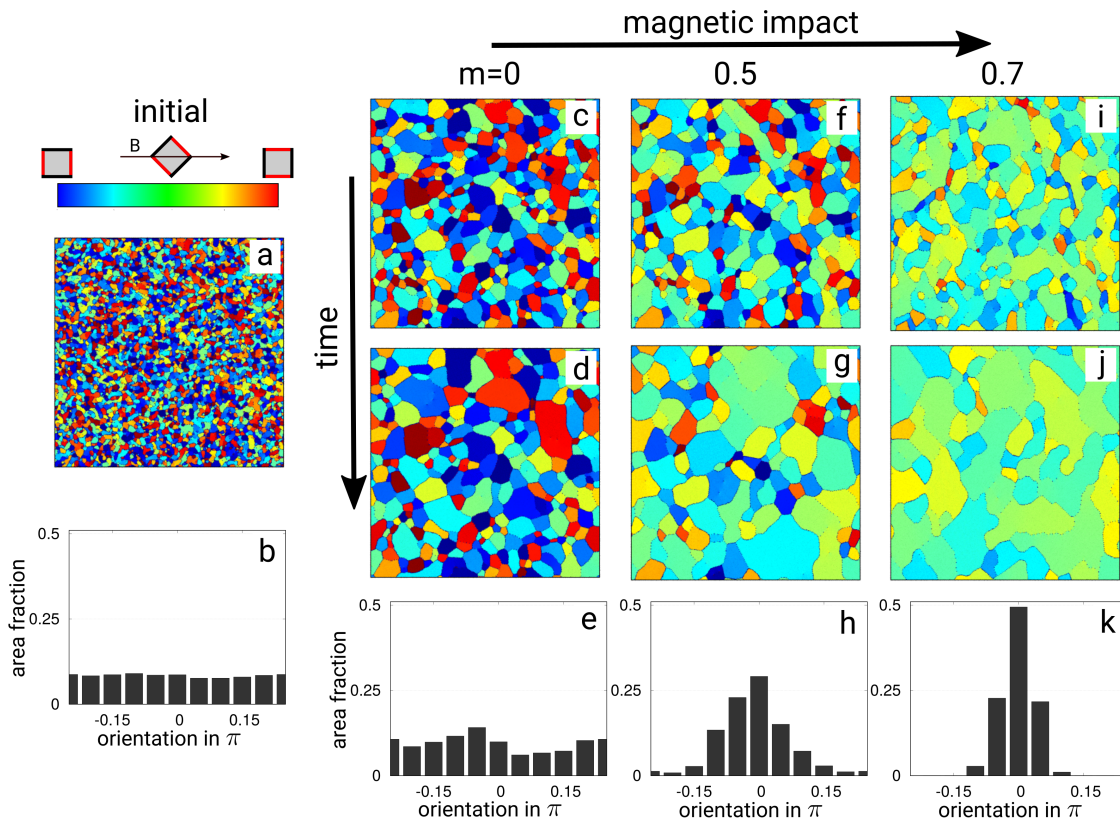


FIG. 2. Grain structure during annealing. The color represents the local orientation w.r.t. the external magnetic field. The area fraction is shown as function of orientation for the initial and final configurations for different magnetic fields m . The times for the snapshots for $m=0, 0.5$ and 0.7 are $(9 \cdot 10^3, 2.7 \cdot 10^4)$, $(1 \cdot 10^3, 1.1 \cdot 10^4)$ and $(4.1 \cdot 10^3, 1.6 \cdot 10^4)$, respectively.

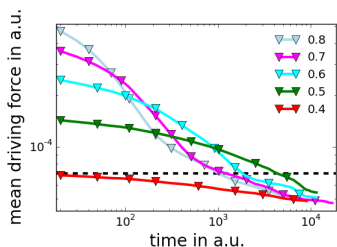


FIG. 3. Mean magnetic force during coarsening for different applied magnetic fields m .

this regime the GSD statistics become more and more noisy. Fluctuations in the GSD approximation increase for larger times and higher magnetic impact. In order to compare the GSD for different external magnetic fields in the limit of large times, we average $\exp(\mu)$ and σ for large times and use the averaged value to reconstruct the log-normal distribution, see Fig. 4. Large external magnetic fields, $m > 0.5$ shift the maximum of the GSD towards smaller sizes. But the tail becomes wider. Thus, the number of large grains w.r.t the average grain size is increased. For smaller external magnetic fields, $m < 0.5$ the tendency is the same but the difference is minor.

D. Grain coordination and shape

Various other geometrical and topological measures have been considered to define the grain structure. We here analyze the next neighbor (coordination number) distribution (NND), the axes ratio (elongation of the grains) distribution (ARD) and the orientation distribution of the small axis (SAOD), measuring the orientation of the elongated grains, see Fig. 5.

We concentrate on the large time distribution for which the coarsening is self similar. Fig. 5 shows the next neighbor distribution (NND), which is also fitted by a log-normal distribution. With increasing external magnetic field the distribution broadens and the maximum is shifted to smaller values. This can already be related to the faster growth, which leads to larger grains and thus also an increased difference in grain size. Classical empirical laws for topological properties in grain structures, such as the Lewis' law and the Aboav-Weair's law, see [23] for a review, show a linear relation between the coordination number and the area of the grains and postulate that grains with high (low) coordination number are surrounded by small (large) grains, respectively. These effects are further enhanced by the elongation of grains, which lead to more neighbors. Additionally, small grains between elongated grains have less neighbors.

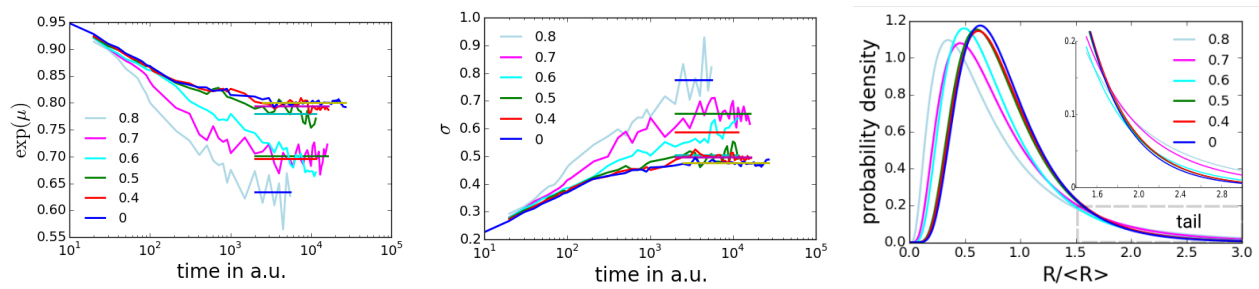


FIG. 4. Log-normal distribution parameters $\exp(\mu)$ and σ over time and GSD for final averaged values for m between $[0; 0.8]$. The data for $m = 0$ correspond with [4] and the experimentally found universal GSD in [1].

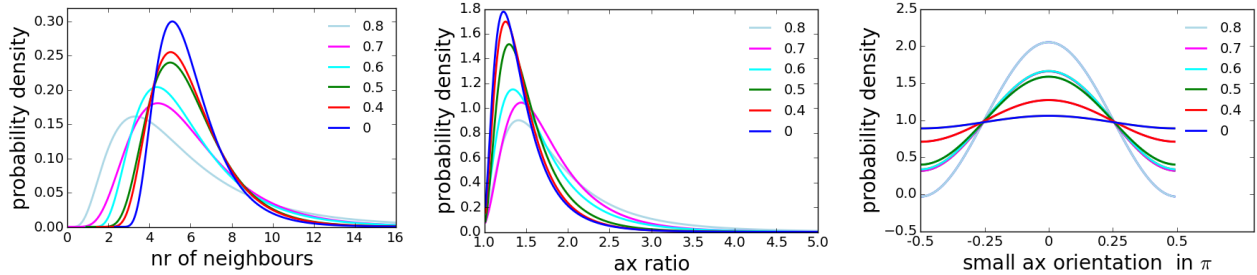


FIG. 5. Log-normal description for next neighbor distribution (NND), axis ratio distribution (ARD) and cosine description for small axis orientation distribution (SAOD), obtained from self similar coarsening regime of converged GSD. m is varied between $[0; 0.8]$.

The elongation of a grain is measured by approximating the grain by an ellipse. The ratio between the long and short axis then describes the elongation. The axes ratio distribution (ARD) can again be approximated by a log-normal distribution, Fig. 5. With increasing magnetic impact the ratio increases and more and more elongated grains are present. The orientation of the elongation is correlated with the external magnetic field. In Fig. 5 the orientation distribution of the small axes with the direction of the external magnetic field (SAOD) is shown. Here the distribution is approximated by a cosine. The elongated grains become more and more oriented perpendicular to the external magnetic field.

IV. DISCUSSION

Classical Mullins-like models for grain growth predict self similar growth and a scaling law t^α for the average radius with $\alpha = 1$ [6]. This also does not change if external magnetic fields are introduced as an additional driving force. In contrast to our simulation, see Fig. 1, no influence of the scaling behavior is observed. Even though the texture depends on strength and direction of the external magnetic field [24–29]. In these simulations the increase of growth of well aligned grains is leveled by the decrease of growth of not well aligned grains, which leads to independent scaling on the additional driving force. However, in experiments mostly smaller exponents are observed. The scaling typically depends on process pa-

rameters and for long times the grain growth stagnates. To achieve these effects in simulations requires additional retarding or pinning forces.

Within the considered PFC model triple point and orientational pinning are naturally present, which is one reason for the observed lower scaling exponent and the stagnation. External magnetic fields introduce an additional driving force to the system. If large enough they can overcome the retarding forces and enhance growth. This explains the dependent growth regime with scaling exponents depending on the applied magnetic field. If the magnetic driving force is large enough all retarding forces can be overcome and an exponent of $\alpha = 1$ reached.

Grain growth under an applied magnetic field leads to preferable growth of well aligned grains. It is this grain selection which decreased the magnetic driving force over time. If the texture is dominated by well aligned grains, the magnetic driving force is no longer a function of the applied field but is limited by the texture, see Fig. 3. Only parts of the retarding forces can be overcome and the scaling becomes independent on the magnetic interaction. Turning off the magnetic field in this regime of well aligned grains leads to stagnation. It can only be speculated about the origin of this retarding forces and the mechanism they are overcome by the magnetic field. But, crystalline defects and elastic properties are known to be modified by the local magnetization [18] and lead to magnetization dependent mobilities. The same mechanism may also open new reaction paths for defect movement which might remove the retarding forces.

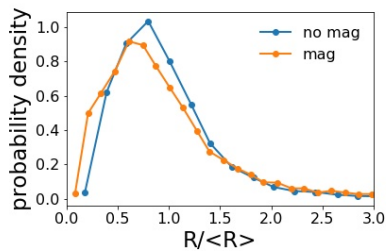


FIG. 6. GSD of Zr sheet after annealing with and without magnetic fields of 19 T. Data is extracted from Fig. 14 in [30]. The mean grain size $\langle R \rangle$ is $10\mu\text{m}$ for the sample annealed without magnetic field and $18\mu\text{m}$ for the sample annealed with magnetic field.

In the case of small magnetic field the coarsening stagnates. In this regime the magnetic impact is not large enough to overcome the retarding force responsible for stagnation.

Within the independent scaling regime self similar growth is observed which allows to compute various geometrical and topological properties of the grain structure. Their dependence on the magnitude of the applied magnetic field has been analyzed. The considered grain size distribution (GSD), next neighbor distribution (NND) and axes ratio distribution (ARD) broaden with increasing m , leading to larger grains, more grains with very few and many neighbors and more elongated grains, see Figs. 4 and 5. The shift in the NND to smaller coordination number has also been reported for simulations based on Mullins type models [26].

Even though, texture control by magnetic fields is of increasing interest [14] there are not many data on the influence of magnetic fields on GSD in thin films available. In [30] the texture and grain size evolution of thin Zr sheets annealed with and without magnetic fields at different temperatures are studied. Increasing temperature and applying external magnetic fields lead

to increasing mean size of the grains. The orientation of the final grains are influenced by the magnetic field and the orientation distribution becomes peaked at favorable orientations. The same tendency as predicted by our simulations, Fig. 2. In Fig. 6 the GSD are compared for these samples after annealing with and without magnetic field. The magnetic field shifts the peak of the GSD towards smaller values leading to an increase of relatively small grains and relatively large grains. The GSD also widens and the tail is increased by the magnetic field. Also these details in the evolution follow qualitatively our simulation results, Fig. 4. But we are not aware of an experimental study showing the increased elongation of the grains perpendicular to the external magnetic field.

V. CONCLUSION

Magnetic enhanced annealing accelerate coarsening. Due to the additional driving force induced by the magnetic anisotropy grains aligned preferably grow at the expense of the other. This leads to grain selection and a texture dominated by well aligned grains. As the amount of similar oriented grains increase the mean orientation difference between grains decreases. Thus, also the mean magnetic driving force decreases with time due to texture change. The scaling exponent becomes independent for large times for large enough magnetic interaction.

But not only the scaling changes also characteristic geometric and topological properties are influenced by the applied magnetic field.

ACKNOWLEDGMENTS

A.V. and R.B. acknowledge support by the German Research Foundation (DFG) under Grant No. Vo899/21 in SPP1959. We further acknowledge computing resources provided at Jülich Supercomputing Center under Grant No. HDR06.

-
- [1] K. Barmak, E. Eggeling, D. Kinderlehrer, R. Sharp, S. Ta'asan, A. Rollett, and K. R. Coffey, *Prog. Mat. Sci.* **58**, 987 (2013).
 - [2] K. R. Elder, M. Katakowski, M. Haataja, and M. Grant, *Phys. Rev. Lett.* **88**, 245701 (2002).
 - [3] K. R. Elder and M. Grant, *Phys. Rev. E.* **70**, 051605 (2004).
 - [4] R. Backofen, K. Barmak, K. R. Elder, and A. Voigt, *Acta Mater.* **64**, 72 (2014).
 - [5] W. Mullins, *J. Appl. Phys.* **27**, 900 (1956).
 - [6] W. W. Mullins, *Acta Materialia* **46**, 6219 (1998).
 - [7] K. Barmak, J. Kim, C. Kim, W. Archibald, G. Rohrer, A. Rollett, D. Kinderlehrer, S. Ta'Asan, H. Zhang, and D. Srolovitz, *Scr. Mater.* **54**, 1059 (2006).
 - [8] E. A. Holm and S. M. Foiles, *Science* **328**, 1138 (2010).
 - [9] P. Streitenberger and D. Zöllner, *Acta Mater.* **78**, 184105114 (2014).
 - [10] M. Upmanyu, D. Srolovitz, A. Lobkovsky, J. Warren, and W. Carter, *Acta Mater.* **54**, 1707 (2006).
 - [11] G. Toth, T. Pusztai, and L. Granasy, *Phys. Rev. B* **92**, 184105 (2015).
 - [12] S. Esedoglu, *Comput. Mater. Sci.* **121**, 209 (2016).
 - [13] G. La Boissoniere, R. Choksi, K. Barmak, and S. Esedoglu, *Materialia* **6**, 100280 (2019).
 - [14] S. Rivoirard, *JOM* **65**, 901 (2013).
 - [15] O. Guillon, C. Elsässer, O. Gutfleisch, J. Janek, S. Korte-Kerzel, D. Raabe, and C. A. Volkert, *Materials Today* **21**, 527 (2018).
 - [16] N. Faghihi, N. Provatas, K. R. Elder, M. Grant, and M. Karttunen, *Phys. Rev. E* **88**, 032407 (2013).
 - [17] M. Seymour, F. Sanches, K. R. Elder, and N. Provatas, *Phys. Rev. B* **92**, 184109 (2015).

- [18] R. Backofen, K. R. Elder, and A. Voigt, *Physical Review Letters* **122**, 126103 (2019).
- [19] M. Greenwood, N. Provatas, and J. Rottler, *Phys. Rev. Lett.* **105**, 045702 (2010).
- [20] N. Ofori-Opoku, J. Stolle, Z.-F. Huang, and N. Provatas, *Phys. Rev. B* **88**, 104106 (2013).
- [21] R. Backofen, A. Rätz, and A. Voigt, *Philos. Mag. Lett.* **87**, 813 (2007).
- [22] S. Praetorius and A. Voigt, *SIAM J. Sci. Comput.* **37**, B425 (2015).
- [23] S. Chiu, *Material Characterization* **34**, 149 (1995).
- [24] D. A. Molodov, P. J. Konijnenberg, L. A. Barrales-Mora, and V. Mohles, *Journal of Materials Science* **41**, 7853 (2006).
- [25] L. A. Barrales-Mora, V. Mohles, P. J. Konijnenberg, and D. A. Molodov, *Computational Materials Science* **39**, 160 (2007).
- [26] D. A. Molodov, C. Bollmann, P. J. Konijnenberg, L. A. Barrales-Mora, and V. Mohles, *Materials Transactions* **48**, 2800 (2007).
- [27] H. C. Lei, X. B. Zhu, Y. P. Sun, L. Hu, and W. H. Song, *Europhys. Lett.* **85**, 38004 (2009).
- [28] J. B. Allen, *Journal of Engineering Materials and Technology* **138**, 041012 (2016).
- [29] P. E. Goins, H. A. Murdoch, E. Hernández-Rivera, and M. A. Tschopp, *Computational Materials Science* **150**, 464 (2018).
- [30] D. A. Molodov and N. Bozzolo, *Acta Materialia* **58**, 3568 (2010).